Letter | Editors' Suggestion

Laser-based approach to verify nuclear excitation by electron capture

Jintao Qi [1,2,*] Boqun Liu [1,*] and Xu Wang [1,3,†]

[1]*Graduate School, China Academy of Engineering Physics, Beijing 100193, China*

[2]*College of Engineering Physics, Shenzhen Technology University, Shenzhen 518118, China*

[3]*Southern Center for Nuclear-Science Theory, Institute of Modern Physics, Chinese Academy of Sciences, Huizhou, Guangdong 516000, China*

(Received 19 November 2023; revised 1 September 2024; accepted 25 September 2024; published 12 November 2024)

Nuclear excitation by electron capture (NEEC) is a theoretically envisioned yet experimentally unverified process that intricately links nuclear and electronic degrees of freedom. For nearly five decades, the experimental validation of NEEC has remained elusive, primarily hindered by challenges in excitation and detection methodologies. This study proposes a laser-based strategy for verifying NEEC, exploiting the isomeric excitation of the ^{235}U nucleus within a laser-cluster interaction scheme. With proper laser parameters, NEEC overwhelmingly dominates, constituting over 99.9% of the isomeric excitation yield. The long lifetime of the ^{235}U isomer allows detection without interfering atomic background. Additionally, distinctive dependencies of isomeric excitation yield on laser parameters provide further confirmation for the NEEC mechanism.

DOI: 10.1103/PhysRevC.110.L051601

Introduction. An atomic nucleus can undergo excitation through the energy released in a downward electronic transition. This phenomenon is termed nuclear excitation by electron capture (NEEC) when the electronic transition occurs from a free state to a bound state [1–6]. For bound-bound electronic transitions, it is referred to as nuclear excitation by electron transition (NEET) [7–12], while free-free electronic transitions are denoted as nuclear excitation by inelastic electron scattering (NEIES) [13–17]. These processes, facilitating the interaction of nuclear and electronic degrees of freedom, play a crucial role in actively controlling nuclear states.

Among these processes, NEEC stands out as the only one lacking experimental validation, despite theoretical proposals spanning nearly half a century [1]. Recent experimental efforts are based on accelerators and the ^{93}Mo nucleus. However, two similar experiments have yielded conflicting results (experiments [18,19], calculations and analyses [20–22]). Alternative prospects for NEEC verification using electron beam ion traps (EBIT) have been suggested [23,24]. The definitive validation of NEEC remains an active area of interest, representing a significant contemporary challenge in the field.

Verifying NEEC presents challenges in both the excitation and detection phases. First, in excitation, achieving exclusive or predominantly NEEC-induced nuclear excitation, with minimal interference from alternative mechanisms, is intricate. For example, in the ^{93}Mo experiments [18,19], calculations reveal that Coulomb excitation from positive ions can surpass NEEC by several orders of magnitude [18,20–22]. In plasma environments, NEEC contends with major competition from NEIES, particularly as NEIES operates across a broader range of electron energies. Second, in the detection phase, confirming NEEC occurrences proves nontrivial. Proposals reliant on EBIT encounter challenges discerning weak nuclear-decay signals amidst the more robust background of atomic processes [23,24]. Furthermore, the number of trapped ions in an EBIT is usually insufficient for detectable isomeric excitation.

In this Letter we propose a viable approach for verifying NEEC that addresses the existing challenges. Our strategy is based on laser-matter interaction, instead of accelerators. Specifically, we exploit the interaction between intense femtosecond laser pulses and ^{235}U clusters, and demonstrate that under suitable laser parameters the isomeric excitation of ^{235}U nuclei predominantly occurs via NEEC, with minimal contribution ($<0.1\%$) from alternative mechanisms. The ^{235}U isomer, with a 26-minute lifetime primarily governed by internal conversion (IC), allows for efficient detection using a multichannel plate detector. The long lifetime diminishes atomic processes disturbing the detection. By scrutinizing the isomer signal's dependence on laser parameters, such as intensity, wavelength, and pulse duration, we can unequivocally confirm NEEC, as distinct mechanisms exhibit unique laser-parameter dependencies.

This proposal stems from an in-depth comprehension of two key aspects: (a) the intricacies of the laser-cluster interaction process and (b) the processes governing the nuclear isomeric excitation of ^{235}U. Subsequent sections will elucidate these two aspects.

Laser-cluster interaction and cluster expansion. We examine the interaction between an intense femtosecond laser pulse and an ^{235}U atomic cluster. Our analysis assumes a cluster containing 10^6 atoms (notably, the discussion and conclusion

*These authors contributed equally to this work.

†Contact author: xwang@gscaep.ac.cn

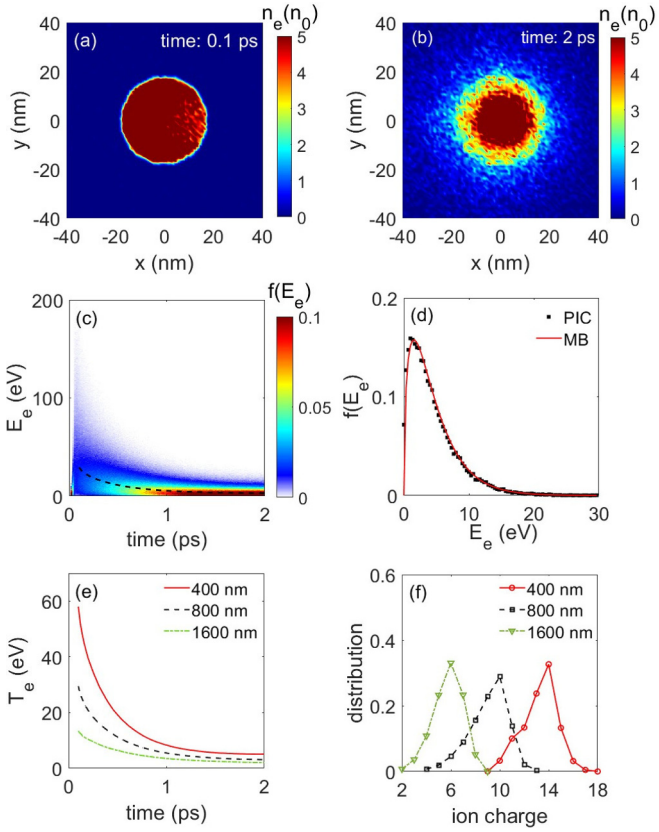

FIG. 1. (a) Electron density distribution immediately after irradiating the cluster with an intense laser pulse of 800 nm wavelength, 30 fs duration, and peak intensity 5×10^{15} W/cm^2. (b) Electron density distribution at 2 ps during the cluster expansion. Electron densities are presented in units of n_0, the atomic number density of ^{235}U. (c) Temporal evolution of the electron kinetic energy distribution in the cluster. The color bar represents the value of the normalized energy distribution function $f(E_e)$. The black dashed curve indicates the electron temperature. (d) Comparison of the electron kinetic energy distribution at 2 ps with a Maxwell-Boltzmann distribution of temperature 3 eV. (e) Evolution of electron temperature for three different laser wavelengths, with the laser pulses having the same duration and peak intensity as specified above. (f) Ion charge distributions for different laser wavelengths at 2 ps.

are independent of the cluster size, as shown later). Given the density of ^{235}U (19.1 g/cm^3, number density $n_0 = 4.69 \times 10^{22}$ cm^{-3}), the radius of the cluster is 17.2 nm.

The intense laser pulse induces ionization in the constituent atoms, causing the release of electrons from each atom [25,26]. The degree of ionization is determined by laser parameters. The liberated electrons predominantly remain within the cluster, forming a nanoplasma ball with solid-state density [27]. For instance, Fig. 1(a) illustrates the electron density distribution immediately after irradiation by a laser pulse with wavelength 800 nm, pulse duration 30 fs (FWHM for intensity), and peak intensity 5×10^{15} W/cm^2. Subsequently, the cluster undergoes expansion due to hydrodynamic pressure from the electrons and Coulomb repulsion from the ions. This expansion lasts for a few picoseconds, during which electrons collide with and excite the nuclei. Figure 1(b) depicts the electron density distribution at 2 ps during the cluster expansion, revealing a persistent high-density core despite the cluster's enlargement. Notably, the majority of electrons remain confined within the cluster. Eventually (around 10 ps), the cluster fully dissociates into electrons and ions, which can be directed toward the detector.

The interaction between the laser and the cluster, as well as the dynamics of cluster expansion, are calculated using the standard 2D3V (two dimensions in space and three dimensions in velocity) particle-in-cell (PIC) simulation with the EPOCH code (version 4.18) [28–30]. The simulation box has dimensions of 2 μm × 2 μm, with a mesh size of 1 nm × 1 nm. Both laser-field ionization and electron collisional ionization are included.

The electron energies are recorded at each time step. In Fig. 1(c), the time-dependent electron energy distribution in the cluster is illustrated. Given the extremely short electron relaxation time (on the order of 0.1 fs [31,32]), the electron energy distribution essentially resembles a thermal distribution at each time, allowing for the extraction of a temperature. The black dashed curve represents the time-dependent electron temperature, reaching its highest value immediately after the laser pulse irradiation (29.5 eV at 0.1 ps) and gradually decreasing as the cluster expands. Figure 1(d) compares the electron kinetic energy distribution at 2 ps with a Maxwell-Boltzmann distribution of temperature 3 eV.

The electron temperature exhibits a sensitive dependence on laser parameters, especially the wavelength. In Fig. 1(e), the evolution of the electron temperature is depicted for three wavelengths—400, 800, and 1600 nm—while maintaining the pulse duration and peak intensity constant. Notably, shorter wavelengths result in higher temperatures. The temperatures for 400 nm (1600 nm) are approximately 2 (0.45) times those for 800 nm. This phenomenon arises from the enhanced penetration of shorter wavelengths through the high-density plasma, leading to increased energy deposition into the cluster. Similar findings have also been reported in the literature [33–36]. Furthermore, lasers with different wavelengths yield distinct ion charge distributions, as depicted in Fig. 1(f). Shorter-wavelength lasers generate higher ion charge states. (Effects of recombination on ion charge states have been calculated, as detailed in the Supplemental Material (SM) [37].) Therefore efficient control of the nanoplasma and the underlying nuclear excitation mechanism can be achieved by adjusting the laser parameters, as elucidated in the subsequent discussion.

Nuclear excitation in the cluster. We investigate the excitation of the ^{235}U nucleus from its ground state (spin-parity $1/2^+$) to the low-lying 76.7-eV isomeric state (spin-parity $7/2^-$) [38–41]. Designated as ^{235m}U, this isomeric state is the second-lowest nuclear excited state among all known nuclei (the lowest being the isomeric state of ^{229}Th with an energy of 8.3 eV [42]). The transition between the nuclear ground state and the isomeric state is of type $E3$. The isomeric state decays into the ground state almost solely through IC with a half-life of 26 minutes. The reason to choose ^{235}U is attributed to its low isomeric transition energy such that a moderately intense laser is capable of exciting the nucleus, and to its higher

abundance compared to ^{229}Th. No other nuclear excited states are known to have energies below 1 keV.

In a laser-heated cluster nanoplasma, multiple nuclear excitation mechanisms are possible. Electronic excitation processes include NEEC, NEIES, and NEET. Optical excitations can occur through blackbody radiation, bremsstrahlung, and the intense laser pulse itself. Notably, NEEC and NEIES significantly surpass NEET and optical excitations, exhibiting magnitudes higher. Calculation results for the latter, weaker, processes are provided in the SM [37]. The distinguishing factor in laser-heated clusters is the solid-state high electron density, a key difference from conventional laser-generated plasmas with substantially lower electron densities, where NEET might dominate [43]. This distinction is evident in the following analysis: under identical temperatures, if the plasma density increases by a factor of N (electron density $n_e \to Nn_e$ and ion density $n_i \to Nn_i$), then the probability of NEEC or NEIES increases by N^2 times (the electron flux becoming N times and the number of nuclei becoming N times), whereas NEET increases only by N times (relevant to the number of nuclei but not to the electron flux). Optical excitation from blackbody radiation scales linearly with N, and from bremsstrahlung as N^2; however, optical excitation is a comparatively weak process and can be disregarded. Consequently, the laser-cluster approach strongly favors NEEC and NEIES over competing mechanisms, especially NEET.

To accentuate NEEC over its main competitor NEIES, proper laser parameters must be used such that the electron temperature in the cluster nanoplasma favors NEEC over NEIES. As NEEC operates at electron energies below the isomeric energy of 76.7 eV, while NEIES operates at higher energies, the strategy involves maintaining a low electron temperature. This typically implies using lower-intensity and longer-wavelength laser pulses, as shown above. However, the situation is a little more complicated.

Low-intensity lasers yield relatively low ion charge states, requiring higher electron energies to initiate NEEC. For instance, with U^{3+}, NEEC initiation demands an electron kinetic energy of at least 56.9 eV, given the ionization potential of the third electron (19.8 eV). However, a thermal distribution reaching 56.9 eV also extends noticeably above 76.7 eV, contributing significantly to NEIES. Higher charge states (e.g., U^{8+}) are necessary to provide recombining energy levels deep enough for efficient utilization of low-energy electrons, requiring however higher laser intensities. Thus, a meticulous exploration is essential to identify a laser intensity range high enough to create relatively highly charged ions while concurrently maintaining the electron temperature significantly below 76.7 eV. Fortunately, such a laser intensity range exists for ^{235}U.

Now, let us elucidate the procedure for calculating nuclear isomeric excitation. The isomer production yield per cluster is expressed as

$$Y_{\rm exc}(t) = 4\pi \int_0^t dt' \int_0^\infty r^2 dr\, n_i(r,t') n_e(r,t') \times \sum_q P_q(t') \left[\langle \sigma^q_{\rm NEEC} v \rangle (t') + \langle \sigma^q_{\rm NEIES} v \rangle (t') \right], \quad (1)$$

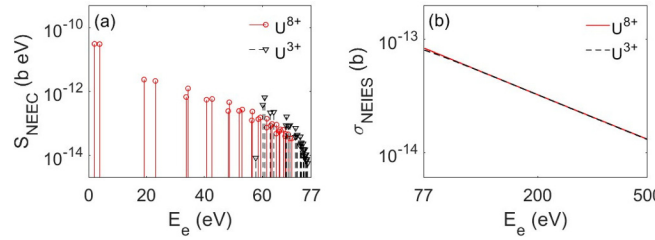

FIG. 2. (a) NEEC resonant strength $S_{\rm NEEC}$ for U^{3+} and U^{8+}. The 30 most significant NEEC channels are displayed for each ionic state. U^{3+} requires higher electron energies to initiate NEEC due to less deeply bound levels. (b) NEIES cross section $\sigma_{\rm NEIES}$ for the same U^{3+} and U^{8+} ionic states. Note that NEEC occurs below the isomeric energy of 76.7 eV, while NEIES occurs above this energy.

where $n_i(r,t)$ and $n_e(r,t)$ denote the time-dependent density of ^{235}U ions and electrons, respectively. $P_q(t)$ represents the time-dependent probability of the charge state U^{q+}. $\sigma^q_{\rm NEEC}$ ($\sigma^q_{\rm NEIES}$) denotes the NEEC (NEIES) cross section for U^{q+}. $\langle \sigma^q_{\rm NEEC} v \rangle (t)$ is the NEEC reaction rate, obtained by averaging over the electron velocity distribution at time t:

$$\langle \sigma^q_{\rm NEEC} v \rangle (t) = \int dE_e f(E_e,t) v(E_e) \sigma^q_{\rm NEEC}(E_e) \quad (2)$$

$$= \sum_k f(E_k,t) v(E_k) S^q_{\rm NEEC}(E_k). \quad (3)$$

The NEEC cross section is integrated over energy, giving the resonant strength $S^q_{\rm NEEC}$ under an isolated resonance approximation. NEEC channels are labeled by k, and E_k represents the corresponding energy of the free electron. $v(E_e)$ denotes the electron velocity corresponding to the kinetic energy E_e. The NEIES reaction rate $\langle \sigma^q_{\rm NEIES} v \rangle (t)$ follows an expression similar to Eq. (2).

Exemplary $S^q_{\rm NEEC}$ and $\sigma^q_{\rm NEIES}$ are illustrated in Fig. 2 for two ionic states, U^{3+} and U^{8+}. The NEEC resonant strength exhibits discrete energies below the isomeric energy of 76.7 eV, whereas the NEIES cross section is defined on continuous energies above the isomeric energy. While $S^q_{\rm NEEC}$ differs significantly for each ionic state due to specific bound levels, $\sigma^q_{\rm NEIES}$ is generally very similar for different ionic states [17]. These cross-section calculations are based on a Dirac distorted wave Born approximation, and the electron wave functions are computed using the openly accessible code RADIAL [44]. The reduced nuclear transition probability is taken to be $B(E3, {\rm g} \to {\rm is}) = 0.009$ W.u. (equivalently 0.036 W.u. is $\to$ g) [45]. Using this B value the half-life of the isomeric state is calculated to be 3.4×10^3 s, roughly within a factor of two compared to the experimental value of 1.6×10^3 s [38]. The calculated IC coefficient is 1.9×10^{20}, which is approximately half the value of 4.4×10^{20} from Ref. [45], and it is also consistent to an early estimation [46] and experiment [40]. The difference is mainly from the calculation of multi-electron wave functions. For more details on the theoretical framework and additional results for different ionic states, refer to the SM [37].

We calculated the isomer production yield per cluster under varying laser parameters. Figure 3(a) shows the isomer

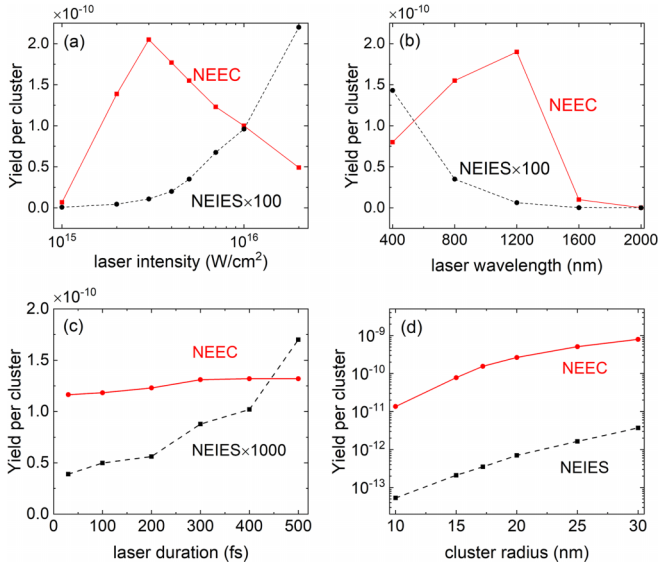

FIG. 3. (a) Isomer production yield per cluster as a function of laser intensity. The laser wavelength is 800 nm and the pulse duration is 30 fs. Note that the NEIES yield has been multiplied by 100 for the purpose of display. (b) Isomer production yield per cluster for different laser wavelengths. The laser intensity is fixed at 5×10^{15} W/cm^2 and the pulse duration is 30 fs. (c) Isomer production yield per cluster for a fixed laser pulse energy but different pulse durations. The laser wavelength is 800 nm. A shorter (longer) pulse duration corresponds to a higher (lower) peak intensity. (d) Isomer production yield per cluster for various cluster sizes. The laser wavelength is 800 nm, peak intensity is 5×10^{15} W/cm^2, and pulse duration is 30 fs.

production yield (at 5 ps when the cluster expansion and nuclear excitation process is mostly over) as a function of laser intensity for NEEC and NEIES, with laser wavelength 800 nm and pulse duration 30 fs. Note that the NEIES yield has been multiplied by 100 for clarity, so the NEEC yield is much (two or three orders of magnitude) higher than the NEIES yield. Around an intensity of 3×10^{15} W/cm^2, the NEEC yield exceeds the NEIES yield by over 1000 times, signifying that NEEC accounts for over 99.9% of the isomeric excitation. Additionally, NEEC and NEIES exhibit distinct intensity dependencies: NEEC exhibits a peak around 3×10^{15} W/cm^2, while NEIES shows a monotonic increase with laser intensity. This distinctive behavior can serve as an additional confirmation of the NEEC mechanism in experiments.

In Fig. 3(b), the isomer production yield is presented as a function of laser wavelength, with a fixed laser intensity of 5×10^{15} W/cm^2 and a pulse duration of 30 fs. Across the entire wavelength range from 400 to 2000 nm, the NEEC yield consistently surpasses the NEIES yield by two to three orders of magnitude. Furthermore, NEEC and NEIES exhibit distinctive dependencies on laser wavelength. NEEC reaches a peak around 1200 nm, while NEIES decreases steadily with increasing wavelength.

In Fig. 3(c), the isomer production yield is depicted as a function of laser pulse duration, while keeping the laser pulse energy constant. Such a pulse compression or stretching can be performed in experiments. The laser wavelength is set to 800 nm. The laser peak intensity is higher (lower) for a shorter (longer) pulse duration. For this illustration, the peak intensity is 2×10^{15} W/cm^2 for a duration of 30 fs and 1.2×10^{14} W/cm^2 for a duration of 500 fs. Notably, across almost all pulse durations, the NEEC yield consistently exceeds the NEIES yield by over 1000 times. Additionally, NEEC and NEIES display distinctive dependencies on the laser pulse duration. The NEEC yield remains relatively insensitive to pulse duration, while the NEIES yield increases with longer pulse durations.

In Fig. 3(d), the dependence of NEEC and NEIES on the cluster radius is demonstrated. With a fixed laser wavelength of 800 nm, peak intensity of 5×10^{15} W/cm^2, and pulse duration of 30 fs, it is evident that the NEEC yield consistently exceeds the NEIES yield by over two orders of magnitude across varying cluster radii. Importantly, the ratio between NEEC and NEIES remains relatively constant for different cluster sizes.

Discussions.

(a) While experimentally it is more convenient to generate plasmas through direct laser ablation on a solid surface [43,47,48], cluster nanoplasmas offer essential advantages for NEEC verification. As detailed earlier, cluster nanoplasmas exhibit a high, solid-state electron density crucial for emphasizing NEEC and NEIES over competing mechanisms. In contrast, laser-ablated plasma manifests a complex, spatially varying electron density distribution originating from the solid surface. This complexity extends to the electron temperature, a critical factor in distinguishing NEEC from NEIES. In essence, cluster nanoplasma is a "simpler" system compared to surface plasma, and this simplicity is precisely what facilitates the verification of NEEC.

(b) Consider a Gaussian beam profile for a laser pulse, where the focal volume is given by $V_{\rm foc} = 16E^2/\pi\lambda I^2\tau^2$. Here, E represents the pulse energy, λ is the wavelength, I is the peak intensity, and τ is the pulse duration. Using the values $E = 3$ J, $\lambda = 800$ nm, $I = 3 \times 10^{15}$ W/cm^2, and $\tau = 30$ fs, the resulting focal volume is $V_{\rm foc} = 72$ cm^3, which is large enough to contain a sufficient number of ^{235}U clusters. Assuming the delivery of 50 μg of ^{235}U clusters (equivalent to 1.3×10^{17} atoms or 1.3×10^{11} clusters) to the laser focus via a buffer gas, the number of excited ^{235}U nuclei would be approximately $1.3 \times 10^{11} \times 2 \times 10^{-10} \approx 26$ after the interaction. Assuming a laser repetition rate of 10 Hz and a data collection time of 1 min, the number of isomers would be $26 \times 10 \times 60 = 15\,600$. The ^{235}U ions can be guided to a multichannel plate detector, where they are neutralized by the detector electrons. The neutralization occurs rapidly (much less than 1 s). Then the IC process will happen for those nuclei in the isomeric state, releasing electrons and generating currents that can be registered with high efficiency, indicating the number of excited nuclei. Given that the half-life of the excited nuclei via IC is on the order of 10^3 s, approximately ten IC electrons are anticipated every second.

This laser excitation and detection process can be repeated with varying laser parameters to examine parameter dependencies, as anticipated in Figs. 3(a)–3(c). The estimated total quantity of ^{235}U required for these experiments is on the order of 1 g. Despite the anticipated low isomeric excitation probability owing to the $E3$ nature of the transition, the primary criterion for verifying NEEC is the "purity" rather than the excitation efficiency.

(c) Metal clusters can be synthesized using various techniques, including physical, chemical, or biological methods [49,50]. Besides, high-pressure gas jets are employed in the formation of clusters from gases [35]. As illustrated in Fig. 3(d), the ratio between NEEC and NEIES exhibits minimal sensitivity to cluster size, eliminating the requirement for identical cluster sizes.

(d) The potential application of other nuclei, preferably nonradiative ones [51], remains open. As elucidated earlier, the critical factor lies in identifying a suitable synergy between nuclear levels and laser parameters that establishes NEEC as the predominant nuclear excitation mechanism. For nuclear levels with higher energies, x-ray free-electron lasers present a prospective path forward.

(e) Recombination processes are not implemented in the PIC simulations in the current work. We use the corresponding cross sections and the plasma conditions to estimate their effects, which turn out to be minimal for nuclear excitations of ^{235}U, as shown in Sec. 4 of the SM [37]. However, for different nuclei requiring higher plasma temperatures for excitation, these processes might become significant and need to be implemented in the PIC code.

Conclusion. Our proposed laser-cluster interaction method offers a promising route to validate NEEC. The high electron density within the cluster nanoplasma accentuates NEEC and NEIES over other nuclear excitation mechanisms. By adjusting laser parameters, we demonstrate that NEEC overwhelmingly dominates, contributing over 99.9% of the nuclear isomer yield. The distinct dependencies of NEEC on various laser parameters provide a robust foundation for experimental confirmation. Our study not only advances the understanding of nuclear excitation mechanisms but also provides a viable experimental roadmap, offering broader implications for nuclear physics research.

Acknowledgments. We acknowledge funding support from NSAF Grant No. U2330401 and NSFC Grants No. 12147161 and No. 12088101.

[1] V. I. Goldanskii and V. A. Namiot, On the excitation of isomeric nuclear levels by laser radiation through inverse internal electron conversion, Phys. Lett. B **62**, 393 (1976).

[2] N. Cue, J.-C. Poizat, and J. Remillieux, Exciting the nucleus by target electron capture into atomic orbitals, Europhys. Lett. **8**, 19 (1989).

[3] J. Kimball, D. Bittle, and N. Cue, A comment on "nuclear excitation by target electron capture", Phys. Lett. A **152**, 367 (1991).

[4] A. Pálffy, W. Scheid, and Z. Harman, Theory of nuclear excitation by electron capture for heavy ions, Phys. Rev. A **73**, 012715 (2006).

[5] G. Gosselin, V. Méot, and P. Morel, Modified nuclear level lifetime in hot dense plasmas, Phys. Rev. C **76**, 044611 (2007).

[6] J. Gunst, Y. A. Litvinov, C. H. Keitel, and A. Pálffy, Dominant secondary nuclear photoexcitation with the x-ray free-electron laser, Phys. Rev. Lett. **112**, 082501 (2014).

[7] M. Morita, Nuclear excitation by electron transition and its application to uranium 235 separation, Prog. Theor. Phys. **49**, 1574 (1973).

[8] K. Okamoto, Improvement of efficiency of isotope separation using nuclear excitation by electron transition, J. Nucl. Sci. Technol. **14**, 762 (1977).

[9] E. V. Tkalya, Nuclear excitation in atomic transitions (NEET process analysis), Nucl. Phys. A **539**, 209 (1992).

[10] S. Kishimoto, Y. Yoda, M. Seto, Y. Kobayashi, S. Kitao, R. Haruki, T. Kawauchi, K. Fukutani, and T. Okano, Observation of nuclear excitation by electron transition in ^{197}Au with synchrotron x rays and an avalanche photodiode, Phys. Rev. Lett. **85**, 1831 (2000).

[11] S. Kishimoto, Y. Yoda, Y. Kobayashi, S. Kitao, R. Haruki, R. Masuda, and M. Seto, Nuclear excitation by electron transition on ^{197}Au by photoionization around the K-absorption edge, Phys. Rev. C **74**, 031301(R) (2006).

[12] A. Y. Dzyublik, General theory of nuclear excitation by electron transitions, Phys. Rev. C **88**, 054616 (2013).

[13] J. A. Thie, C. J. Mullin, and E. Guth, Electron excitation of nuclei, Phys. Rev. **87**, 962 (1952).

[14] L. I. Schiff, Nuclear multipole transitions in inelastic electron scattering, Phys. Rev. **96**, 765 (1954).

[15] E. V. Tkalya, Excitation of ^{229m}Th at inelastic scattering of low energy electrons, Phys. Rev. Lett. **124**, 242501 (2020).

[16] H. Zhang, W. Wang, and X. Wang, Nuclear excitation cross section of ^{229}Th via inelastic electron scattering, Phys. Rev. C **106**, 044604 (2022).

[17] B. Liu and X. Wang, Isomeric excitation of ^{235}U by inelastic scattering of low-energy electrons, Phys. Rev. C **106**, 064604 (2022).

[18] C. J. Chiara, J. J. Carroll, M. P. Carpenter, J. P. Greene, D. J. Hartley, R. V. F. Janssens, G. J. Lane, J. C. Marsh, D. A. Matters, M. Polasik *et al.*, Isomer depletion as experimental evidence of nuclear excitation by electron capture, Nature (London) **554**, 216 (2018).

[19] S. Guo, B. Ding, X. H. Zhou, Y. B. Wu, J. G. Wang, S. W. Xu, Y. D. Fang, C. M. Petrache, E. A. Lawrie, Y. H. Qiang, Y. Y. Yang, H. J. Ong, J. B. Ma, J. L. Chen, F. Fang, Y. H. Yu, B. F. Lv, F. F. Zeng, Q. B. Zeng, H. Huang *et al.*, Probing ^{93m}Mo isomer depletion with an isomer beam, Phys. Rev. Lett. **128**, 242502 (2022).

[20] Y. Wu, C. H. Keitel, and A. Pálffy, ^{93m}Mo isomer depletion via beam-based nuclear excitation by electron capture, Phys. Rev. Lett. **122**, 212501 (2019).

[21] J. Rzadkiewicz, M. Polasik, K. Słabkowska, L. Syrocki, J. J. Carroll and C. J. Chiara, Novel approach to ^{93m}Mo isomer depletion: Nuclear excitation by electron capture in

resonant transfer process, Phys. Rev. Lett. **127**, 042501 (2021).
[22] S. Guo, Y. Fang, X. Zhou, and C. M. Petrache, Possible overestimation of isomer depletion due to contamination, Nature (London) **594**, E1 (2021).
[23] S. A. Karamian and J. J. Carroll, Possible depletion of isomers in perturbed atomic environments, Laser Phys. **20**, 977 (2010).
[24] K. G. Leach, High-sensitivity nuclear-structure studies of rare isotopes and few-electron systems, DOE Technical Report No. DOE-CSM-17649.
[25] W. Wang, J. Zhou, B. Liu, and X. Wang, Exciting the isomeric ^{229}Th nuclear state via laser-driven electron recollision, Phys. Rev. Lett. **127**, 052501 (2021).
[26] X. Wang, Nuclear excitation of ^{229}Th induced by laser-driven electron recollision, Phys. Rev. C **106**, 024606 (2022).
[27] J. Qi, H. Zhang, and X. Wang, Isomeric excitation of ^{229}Th in laser-heated clusters, Phys. Rev. Lett. **130**, 112501 (2023).
[28] T. D. Arber, K. Bennett, C. S. Brady, A. Lawrence-Douglas, M. G. Ramsay, N. J. Sircombe, P. Gillies, R. G. Evans, H. Schmitz, A. R. Bell, and C. P. Ridgers, Contemporary particle-in-cell approach to laser-plasma modelling, Plasma Phys. Control. Fusion **57**, 113001 (2015).
[29] S. Morris, T. Goffrey, K. Bennett, and T. Arber, Improvements to collisional ionization models for particle-in-cell codes, Phys. Plasmas **29**, 123907 (2022).
[30] M. Afshari, S. Morris, L. Geulig, Z. Chitgar, P. Gibbon, P. Thirolf, and J. Schreiber, The role of collisional ionization in heavy ion acceleration by high intensity laser pulses, Sci. Rep. **12**, 18260 (2022).
[31] L. Spitzer, in *Physics of Fully Ionized Gases* (Interscience, New York, 1967), pp. 76-81.
[32] T. Ditmire, Simulations of heating and electron energy distributions in optical field ionized plasmas, Phys. Rev. E **54**, 6735 (1996).
[33] W. L. Kruer, in *The Physics of Laser Plasma Interactions* (Addison-Wesley, Redwood City, CA, 1988), pp. 168–170.
[34] S. Atzeni and J. Meyer-Ter-Vehn, in *The Physics of Inertial Fusion* (Oxford University Press, Oxford, 2004), pp. 377–380.
[35] S. Erhard, and E. K. U. Gross, Scaling and virial theorems in current-density-functional theory, Phys. Rev. A **53**, R5 (1996).
[36] U. Saalmann, C. Siedschlag and J. M. Rost, Mechanisms of cluster ionization in strong laser pulses, J. Phys. B: At. Mol. Opt. Phys. **39**, R39 (2006).
[37] See Supplemental Material at http://link.aps.org/supplemental/10.1103/PhysRevC.110.L051601 for detailed theoretical framework of calculations and results for minor excitation processes including NEET and photoexcitations, which includes Refs. [52–63].
[38] J. R. Huizenga, C. L. Rao, and D. W. Engelkemeir, 27-minute isomer of U^{235}, Phys. Rev. **107**, 319 (1957).
[39] M. S. Freedman, F. T. Porter, F. Wagner, and P. Day, Transition in 26-min U^{235} of less than 23 electron volts, Phys. Rev. **108**, 836 (1957).
[40] E. Browne and J. K. Tuli, Nuclear data sheets for A = 235, Nucl. Data Sheets **122**, 205 (2014).
[41] F. Ponce, E. Swanberg, J. Burke, R. Henderson, and S. Friedrich, Accurate measurement of the first excited nuclear state in ^{235}U, Phys. Rev. C **97**, 054310 (2018).
[42] S. Kraemer, J. Moens, M. Athanasakis-Kaklamanakis, S. Bara, K. Beeks, P. Chhetri, K. Chrysalidis, A. Claessens, T. E. Cocolios, J. G. M. Correia *et al.*, Observation of the radiative decay of the ^{229}Th nuclear clock isomer, Nature (London) **617**, 706 (2023).
[43] M. R. Harston and J. F. Chemin, Mechanisms of nuclear excitation in plasmas, Phys. Rev. C **59**, 2462 (1999).
[44] F. Salvat and J. M. Fernández-Varea, radial: A Fortran subroutine package for the solution of the radial Schrödinger and Dirac wave equations, Comput. Phys. Commun. **240**, 165 (2019).
[45] J. C. Berengut, Resonant electronic-bridge excitation of the ^{235}U nuclear transition in ions with chaotic spectra, Phys. Rev. Lett. **121**, 253002 (2018).
[46] M. C. Michel, F. Azaro, and I. Perlman, Energy of the isomeric state U^{235m}, Bull. Am. Phys. Soc. Ser. II **2**, 394 (1957).
[47] S. Amoruso, R. Bruzzese, N. Spinelli, and R. Velotta, Characterization of laser-ablation plasmas, J. Phys. B: At. Mol. Opt. Phys. **32**, R131 (1999).
[48] G. Gosselin and P. Morel, Enhanced nuclear level decay in hot dense plasmas, Phys. Rev. C **70**, 064603 (2004).
[49] R. Nagarajan, in *Nanoparticles: Synthesis, Stabilization, Passivation, and Functionalization* (American Chemical Society, Washington, 2008), pp. 2–14.
[50] A. J. Shnoudeh, I. Hamad, R. W. Abdo, L. Qadumii, A. Y. Jaber, H. S. Surchi, and S. Z. Alkelany, in *Biomaterials and Bionanotechnology*, edited by R. K. Tekade (Academic, New York, 2019), pp. 527–612.
[51] J. Feng, W. Wang, C. Fu, L. Chen, J. Tan, Y. Li, J. Wang, Y. Li, G. Zhang, Y. Ma *et al.*, Femtosecond pumping of nuclear isomeric states by the Coulomb collision of ions with quivering electrons, Phys. Rev. Lett. **128**, 052501 (2022).
[52] K. Alder, A. Bohr, T. Huus, B. Mottelson, and A. Winther, Study of nuclear structure by electromagnetic excitation with accelerated ions, Rev. Mod. Phys. **28**, 432 (1956).
[53] J. M. Blatt and V. F. Weisskopf, *Theoretical Nuclear Physics* (Springer, New York, 1979).
[54] M. Rose, *Relativistic Electron Theory* (Wiley, New York, 1961).
[55] H. Zhang and X. Wang, Theory of isomeric excitation of ^{229}Th via electronic processes, Front. Phys. **11**, 1166566 (2023).
[56] H. R. Griem, *Plasma Spectroscopy* (McGraw-Hill, New York, 1994).
[57] P. J. Chantry, Doppler broadening in beam experiments, J. Chem. Phys. **55**, 2746 (1971).
[58] A. Pálffy, J. Evers, and C. H. Keitel, Electric-dipole-forbidden nuclear transitions driven by super-intense laser fields, Phys. Rev. C **77**, 044602 (2008).
[59] J. Gunst, Y. Wu, C. H. Keitel, and A. Pálffy, Nuclear excitation by electron capture in optical-laser-generated plasmas, Phys. Rev. E **97**, 063205 (2018).
[60] H. W. Koch and J. Motz, Bremsstrahlung cross-section formulas and related data, Rev. Mod. Phys. **31**, 920 (1959).
[61] H. A. Kramers, On the theory of X-ray absorption and of the continuous X-ray spectrum, Philos. Mag. **46**, 836 (1923).
[62] Y. Hahn, Electron-ion recombination processes—an overview, Rep. Prog. Phys. **60**, 691 (1997).
[63] Y. Hahn, Plasma density effects on the three-body recombination rate coefficients, Phys. Lett. A **231**, 82 (1997).